JOURNAL OF BIOMATERIALS SCIENCE, POLYMER EDITION, 2017
http://dx.doi.org/10.1080/09205063.2017.1303120

Surface force and vibrational spectroscopic analyses of interfacial water molecules in the vicinity of methoxy-tri(ethylene glycol)-terminated monolayers: mechanisms underlying the effect of lateral packing density on bioinertness

Taito Sekine[a#], Syifa Asatyas[a#], Chikako Sato[b], Shigeaki Morita[c], Masaru Tanaka[b,d] and Tomohiro Hayashi[a,e]

[a]Department of Materials Science and Engineering, Tokyo Institute of Technology, Tokyo, Japan; [b]Department of Biochemical Engineering, Yamagata University, Yamagata, Japan; [c]Department of Engineering Science, Osaka Electro-Communication University, Osaka, Japan; [d]Institute for Materials Chemistry and Engineering, Kyushu University, Fukuoka, Japan; [e]Surface and Interface Science Laboratory, RIKEN, Saitama, Japan

ABSTRACT

Unequivocal dependence of bioinertness of self-assembled monolayers of methoxy-tri(ethylene glycol)-terminated alkanethiol (EG3-OMe SAMs) on their packing density has been a mystery for more than two decades. We tackled this long-standing question by performing surface force and surface-enhanced infrared absorption (SEIRA) spectroscopic measurements. Our surface force measurements revealed a physical barrier of interfacial water in the vicinity of the Au-supported EG3-OMe SAM (low packing density), whereas the Ag-supported one (high packing density) did not possess such interfacial water. In addition, the results of SEIRA measurements clearly exhibited that hydrogen bonding states of the interfacial water differ depending on the substrates. We also characterized the bioinertness of these SAMs by protein adsorption tests and adhesion assays of platelet and human umbilical vein endothelial cells. The hydrogen bonding states of the interfacial water and water-induced interaction clearly correlated with the bioinertness of the SAMs, suggesting that the interfacial water plays an important role determining the interaction of the SAMs with biomolecules and cells.

ARTICLE HISTORY
Received 31 December 2016
Accepted 3 March 2017

KEYWORDS
Bioinertness; oligo(ethylene glycol); self-assembled monolayers; water; surface forces; atomic force microscopy; surface-enhanced infrared adsorption spectroscopy

1. Introduction

Construction of bioinert surfaces to prevent non-specific adsorption or adhesion of proteins and cells is one of pivotal issues in biosensing [1,2], cellular-biological studies [3,4], etc. Self-assembled monolayers (SAMs) of oligo(ethyleneglycol)-terminated molecules (OEG SAMs) have been widely used for a long time because of their high bioinertness as well as easiness of

CONTACT Tomohiro Hayashi hayashi.t.al@m.titech.ac.jp, hayashi@echem.titech.ac.jp
[#]Equally contributed author.

their preparation. Despite a wide spread use of the OEG SAMs, the mechanism underlying their bioinertness has not fully been unveiled, despite much effort devoted thus far [5].

In a field of polymer science, a conventional way to suppress adsorption of biomolecules and adhesion of cells (denoted as bioadhesion, hereafter) is to tailor surfaces with hydrophilic polymers. In such cases, steric repulsion has been a main factor to suppress the bioadhesion. i.e. it is energetically unfavorable from the viewpoints of both entropy and enthalpy for biomolecules and cells to approach the tailored surfaces, since the hydrated polymer chains covering the surfaces have high degrees of freedom in their configurations [6,7]. In contrast to the polymer systems, thiolate molecules in SAMs are densely packed [8–11]. Therefore, the contribution of the steric repulsion cannot be expected in the cases of the SAMs. To clarify the underlying mechanism, many experimental and theoretical studies have been performed to elucidate interfacial behavior of thiolate molecules constituting the SAMs (especially functional terminal groups), ions, and water molecules [5].

Among various OEG SAMs, a SAM of methoxy-tri(ethylene glycol)-terminated alkanethiol (EG3-OMe SAM) is an extensively studied system to understand the mechanism underlying their bioinertness. Here, we review previous works on the EG3-OMe SAMs briefly. Harder et al., for the first time, reported that their bioinertness critically depends on the packing density of the molecules on surfaces (3.6 and 4.2 molecules/nm^2) [12]. Surprisingly, the Au-supported SAM exhibited resistance to the adsorption of fibrinogen, whereas the Ag-supported SAM adsorbed. They reported that the conformations of the EG chains in air are helical and all-trans configurations on Au and Ag, respectively, and speculated that the molecular conformation is the key factor.

Feldman et al. performed the direct measurements of the interaction operating between the EG3-OMe SAMs and fibrinogen immobilized on probes of an atomic force microscope (AFM). They reported that electrostatic (DLVO) repulsion (attraction) operated for the Au- (Ag-) supported SAMs [13]. Their finding was supported by the works by Chan et al., in which the hydroxide ions were preferentially concentrated in the vicinity of the Au-supported SAM by streaming potential measurements [14].

Studies on the interfacial behavior of water molecules were initiated by the computer simulation. The results of their grand canonical Monte Carlo simulation by Pertsin et al. suggested that water molecules penetrated into the Au-supported SAM, whereas the Ag-supported SAM did not allow the penetration of water because of its high molecular packing density [15,16]. This finding was in good agreement with the density profile of water in the interface region measured by neutron reflectivity measurements [17]. We also reported that the Au-supported EG3-OMe and other bioinert SAMs are similarly covered with interfacial water that play a role of a physical barrier to prevent the approach of biomolecules and cells to the surfaces [18].

Collecting together, the interfacial behaviors of the EG chains [12], ions [14,19,20], and water [16,18] strongly depend on the packing density of the EG3-OMe thiolate molecules in the SAMs. Considering the Debye screening length of the experimental conditions of the above experiments (0.7 nm), it is difficult to attribute the origin of bioinertness to electrostatic or electrostatic double layer repulsion induced by the EG3-OMe thiolate molecules, ions and water molecules. We rather strongly expect that physical repulsion induced by the interfacial water molecules is the main factor for the bioinertness. The aim of this work is to clarify the origin of the bioinertness using the well-defined and -studied EG3-OMe SAMs by performing systematic assays of protein adsorption and cell adhesions, since the adsorption and adhesion are governed by different mechanisms. Moreover, we

conduct surface force and surface enhanced infrared absorption (SEIRA) spectroscopic measurements to investigate force induced by the SAMs and hydrogen bonding states of the interfacial water. Combining these results, we discuss the mechanism underlying the bioinertness of the EG3-OMe SAMs.

2. Materials and methods

2.1. Fabrication of SAMs and their substrates

Details of the fabrication process of the Au and Ag film on mica and preparation of SAMs were described elsewhere [18,21]. Both Au and Ag film were prepared by vacuum deposition of gold (99.999%, Furuuchi Chemical Co., Japan) or silver (99.999%, NewMet Ltd., U.K) onto freshly cleaved mica substrates ($10 \times 10 \times 0.3$ mm^3, S & J Trading Inc., NY, U.S.) at 620 K under a vacuum pressure at 10^{-5} –10^{-6} Pa. Then, the Au films were annealed at 620 K in a vacuum chamber for 2 h. To prepare the SAMs, we used 1-octanethiol (Abbreviation: C8, Sigma-Aldrich, U.S-MO) and (1-mercaptoundec-11-yl)tri(ethylene glycol) monomethyl-ether (Abbreviation: EG3-OMe, ProChimia Surfaces, Poland). Both alkanethiol molecules were dissolved in pure ethanol at a concentration of 1 mM. Then, the SAMs were prepared by dipping the metal films into the solutions for 24 h. The SAMs were carefully rinsed with pure ethanol to remove the physisorbed thiol molecules prior to use. The packing density of the SAMs were evaluated by X-ray photoelectron spectroscopy (XPS) (Theta Probe, Thermo Fisher Scientific, MA, U.S.) by measuring the attenuation of the photoelectrons from the substrates (Au_{4f} and Ag_{3d}) [12,18,22].

Static water contact angles of the SAMs were measured by a sessile-drop (5 μL in volume) method (DSA10, Krüss, Hamburg, Germany) at 25 ± 0.5 °C.

2.2. Analysis of protein adsorption

We employed quartz crystal microbalance (QCM) (D300, Q-Sense, Sweden) to measure amounts of fibrinogen adsorbed onto the SAMs. Firstly, gold-coated QCM sensors were cleaned with a UV-O_3 cleaner (UV-300, SUMCO, Japan), and washed by ultrasonic cleaning in acetone, ethanol, and pure water in this order, followed by blow of nitrogen gas. The SAMs were prepared by the same manner that for the Au and Ag substrates. Silver-coated QCM sensors were fabricated by vacuum deposition of silver (99.999%, NewMet Ltd., U.K) with a thickness of 10 nm onto the gold-coated sensors at 313 K in vacuum (10^{-5} –10^{-6} Pa). After the evaporation, the silver-coated sensors were immediately immersed into the thiol solutions. We used human fibrinogen (Biogenesis Ltd., U.K) dissolved in phosphate buffer saline (PBS) at a concentration of 1 mg mL^{-1}. In the QCM measurements, a measurement chamber was filled with PBS. Then, the fibrinogen solution was injected into the chamber. After the resonant frequency of the sensor becomes constant, the PBS solution was injected to the chamber again for rinsing. The amount of the adsorbed fibrinogen was defined as difference in weights before the injection and after rinsing. The conversion from resonant frequency to weight was based on the Sauerbrey equation [23];

$$\Delta m = -\frac{C \cdot \Delta f}{n}, \tag{1}$$

where C = 17.7 ng cm^{-2} Hz^{-1}, Δf is the change in the resonant frequency due to protein adsorption, and the n is the overtone number [(n = 3) in this work] All data were collected

at the $n = 3$ overtone. For the adsorption of soft materials, we frequently need to employ viscoelastic model (Voigt–Voinova model) [24]. However, the trend in the evaluated thickness is same to that in the weights calculated with the Sauerbrey equation. Therefore, we discuss the amount of the adsorbed proteins evaluated by the Sauerbrey model.

2.3. Cell attachment assay

2.3.1. Platelet cells

Details of the platelet attachment assay were described elsewhere [18]. Fresh human blood was mixed with a 1/9 volume of acid citrate dextrose. The mixture was separated to platelet-rich plasma (PRP) and platelet-poor plasma (PPP) by centrifugation. Then, we prepared plasma containing platelet cells at a concentration of 1×10^6 platelet cells mL^{-1} by mixing PRP and PPP. The concentration of the platelet cells in the plasma was determined using a hemocytometer. The 200 μL of the plasma containing platelet cells was placed on the SAMs, and incubated for 60 min at 37 °C. After the incubation, the SAMs were washed three times with PBS. Then, the SAMs were immersed in 1% glutaraldehyde solution for 60 min at 37 °C to fix the adhered platelet cells on the SAMs. The SAMs were washed with PBS, pure water, and ethanol in this order to remove water. The samples were coated with conductive osmium films for the observation with a scanning electron microscope (S-4800, HITACHI, Japan).

2.3.2. Human umbilical vein endothelial cells

Human umbilical vein endothelial cells (HUVECs) were cultured in Dulbecco's Modified Eagle Medium (DMEM/F12, Thermo Fisher Scientific, MA, U.S.) containing 20% of fetal bovine serum (Equitech-Bio, Kerrville, TX, U.S). After confluence was achieved, the cells were washed with PBS, and detached from the cell culture dish (IWAKI, Japan) with 0.25 mg/mL of trypsin solution containing 0.25 mM EDTA. After that, the cells were harvested by centrifugation at 1300 rpm. Cell suspension was prepared by mixing the cell pellet with the cell-culturing medium. Before the cell attachment assay, the SAMs were rinsed with pure ethanol and PBS, respectively. Then, the SAMs were immersed in the cell-culturing medium for overnight at 37 °C. Before the cell attachment assay, the excess medium was discarded from the SAMs.

The cells were seeded on the SAMs at a density of 5.0×10^4 cells cm^{-2}, and cultured for one hour at 37 °C in a CO_2 incubator. After that, the cells were fixed with 4% paraformaldehyde in PBS (Wako, Osaka, Japan) for 10 min at room temperature. After the fixation, the fixed cells were washed three times with PBS, 1% Triton X-100 (MP Biomedicals, Santa Ana, CA, U.S.) in PBS, and 0.02% Tween 20 (MP Biomedicals, Santa Ana, CA, U.S.) in PBS, respectively. The permeabilized cells were incubated with 0.2% anti-vinculin antibody for one hour at 37 °C, and washed three times with the 0.02% Tween 20 in PBS. Then, the cells were incubated with mixed solution containing 0.1% Alexa Fluor 568 goat anti-mouse IgG (for vinculin staining) (Thermo Fisher Scientific, MA, U.S.) and 0.1% Alexa Fluor 488 phalloidin (for actin staining) (Thermo Fisher Scientific, MA, U.S.) for one hour at 37 °C, and washed three times with the Tween 20 in PBS (2 wt%). For staining of nuclei of the cells, ProLong Gold antifade reagent with DAPI (Thermo Fisher Scientific, MA, U.S.) was dropped onto the substrates. We employed a commercial confocal laser scanning microscope system (Olympus, Tokyo, Japan). We prepared three samples for each SAM, and obtained five images at different positions of each SAM substrates. By counting the numbers of cells in the images, we calculated the average densities of the cells.

2.4. Fabrication of colloidal probes

Colloidal probes were prepared by attaching of a washed silica bead (diameter: 18 μm, Duke Sci. Corp., CA, U.S.) to the end of a tipless cantilever (NP-OW, Bruker, MA, U.S., nominal spring constant 0.06 N m^{-1}) using epoxy glue (Araldite, Huntsman Corp., UT, U.S.). The diameters of the beads were determined by optical microscope images prior to the fixation. After the cleaning of the probes with a UV-O_3 cleaner (UV-300, SUMCO, Japan), Au and Ag films and SAMs were fabricated by the same matter for the Au and Ag substrates.

2.5. Surface force measurement

We used a commercial AFM system equipped with a liquid cell (MFP-3D, Oxford Instruments, U.K) to measure the interaction between the SAMs. All force measurements were performed in PBS. Spring constants of the probes were determined from the thermal fluctuation of the probes [25]. Probe velocity on approach and retract was fixed at 200 nm s^{-1}. The reproducibility of the force curves was checked at different positions of the substrates. For the conversion of the deflection of the cantilever to the probe–surface separation, we simply defined a separation of zero as where linearity in the constant compliance region started in the force–displacement curve [18].

2.6. Spectroscopic measurement of the interfacial water molecules by SEIRA spectroscopy

Au and Ag films with a thickness of 20 nm were formed on the flat surface of a hemispherical silicon prism by vacuum deposition. gold (99.999%, Furuuchi Chemical Co., Japan) and silver (99.999%, NewMet Ltd., U.K) were deposited by vacuum deposition with a vacuum chamber (SANYU SVC-700TM, SANYU, Japan) under a vacuum pressure at 4×10^{-4} Pa. The deposition rate of the metals was 0.01 nm s^{-1}. Preparation process of the SAMs was same as that for the metal films. Incident angle of the infrared (IR) beam to the silicon prism was 45°. IR adsorption of the evanescent wave was monitored by Fourier transform infrared spectrometer (Thermo Electron Nexus 470, Thermo Fisher Scientific, MA, U.S.) with liquid nitrogen-cooled HgCdTe detector. For each SAM, we performed SEIRA measurements under dry and wet conditions, respectively. In the wet condition, the spectra were collected during injection of water vapor (relative humidity: 90%) to the measurement cell. Previously, we confirmed that a water layer was formed on the SAMs with a thickness of 5–20 nm by humidity-controlled QCM [19]. IR adsorption spectra of the interfacial water were obtained by subtraction of spectra taken in the wet condition with that in the dry condition.

3. Results and discussion

3.1. Effect of packing density of the alkanethiolates on the protein- and cell-resistance of the Au- and Ag-supported EG3-OMe SAMs

Measured packing density and water contact angle of each SAM were summarized in Table 1. The packing density of the EG3-OMe/Ag SAMs was around 1.3 times higher than that of the EG3-OMe/Au SAMs. This finding is in good agreement with the previous work [26].

Table 1. Packing density and static water contact angle of the EG3-OMe SAMs on Au and Ag ($n = 3$).

SAMs	Packing density (molecules nm^{-2})	Static water contact angle (°)
EG3-OMe/Ag	4.6 ± 0.10	65 ± 2
EG3-OMe/Au	3.5 ± 0.10	65 ± 1

QCM charts and evaluated amounts of adsorbed fibrinogen on the SAMs are shown in Figure 1(A) and (B). The Au-supported SAM showed resistance to the adsorption, whereas the Ag-supported SAM did not, in good agreement with the previous reports [12,26]. A similar trend was found for the SAMs of hydroxy-tetra(ethylene glycol)-terminated alkanethiol (EG4-OH) by Li et al. [27,28]. In their work, they controlled the molecular packing density on Au substrates by using different solutions dissolving the EG4-OH molecules. EG4-OH SAMs exhibited excellent protein resistance at low packing densities, the SAMs lost protein resistance at high packing densities. Together with the results of pervious works, we clearly conclude that the protein resistance of the OEG SAMs strongly depends on their packing density.

Next, we investigated the interaction of the EG3-OMe SAMs with platelet cells. As clearly seen in Figure 2(A), the Au-supported SAM repelled platelet cells. In contrast, the Ag-supported SAM adhered platelet cells. Figure 2(B) displays the detailed pictures of the responses of platelet cells to the SAMs. On the C8 SAM, the shapes of the most of platelet cells become changed from a native biconvex discoid shape to dendritic (early stage of activation) or fully flattened (late stage of the activation). Therefore, the C8 SAM is considered as platelet activating surface (low platelet compatibility). In contrast to the C8 SAM, the Au-supported SAM adheres low density of platelet cells, and the platelet cells were not activated even after adhesion, indicating that the Au-supported EG3-OMe is 'stealth' for platelet cells and its platelet compatibility is high. Several factors to promote the adhesion and activation of platelet cells have been reported, i.e. fibrinogen, its conformational changes, albumin, etc. [29–31]. Previously we evaluated the correlation among adhesion of platelet cells, chemical composition of the surface, water contact angle, and amount of fibrinogen. We concluded that the density of adhered platelet cells correlated quantitatively well with amount of adsorbed fibrinogen. The correlation was also found in this work [Figures 1 and 2(A)].

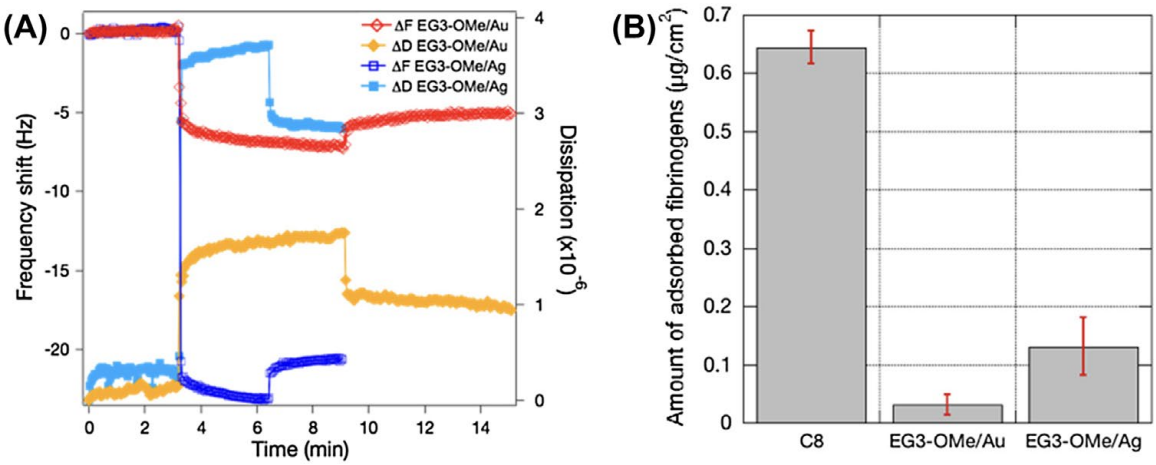

Figure 1. (A) QCM charts (frequency and dissipation) observed for adsorption of fibrinogen onto the Au- and Ag-supported EG3-OMe SAMs. (B) Amount of fibrinogens adsorbed on the SAMs evaluated based on the Sauerbrey equation.
Note: Error bars denote standard deviation ($n = 3$).

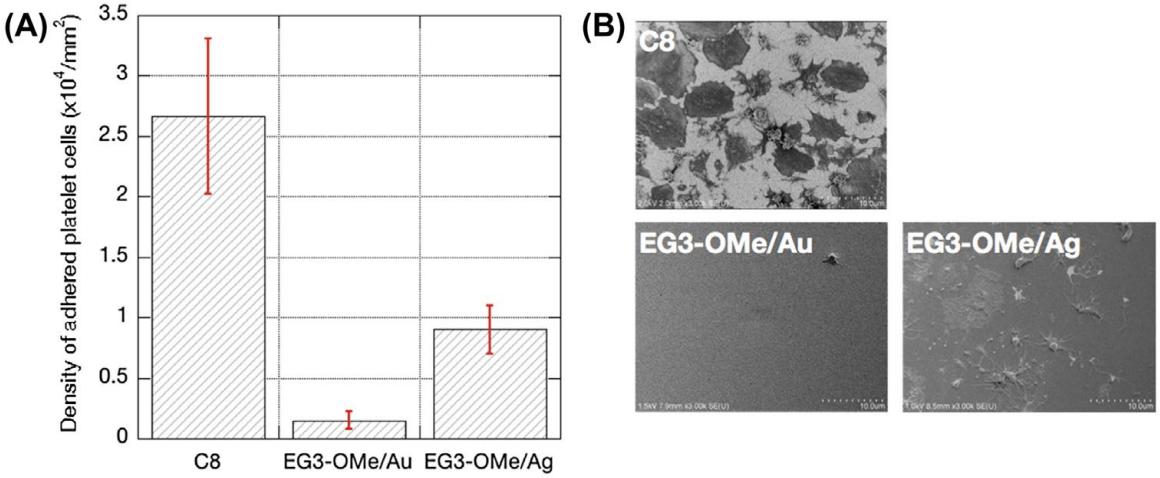

Figure 2. (A) Density of adhered platelet cells on C8, Au- and Ag-supported EG3-OMe SAMs. Error bars denote standard deviation (n = 15). (B) Typical SEM images of the adhered platelet cells on the SAMs.

We also performed the adhesion test of HUVECs onto the SAMs. As shown in Figure 3, the C8 and Ag-supported EG3-OMe SAMs adhered HUVECs, whereas the Au-supported SAMs almost completely suppressed the adhesion. As clearly judged from the fluorescent microscope images [Figure 3(B)], the large footprint area of HUVEC was observed for

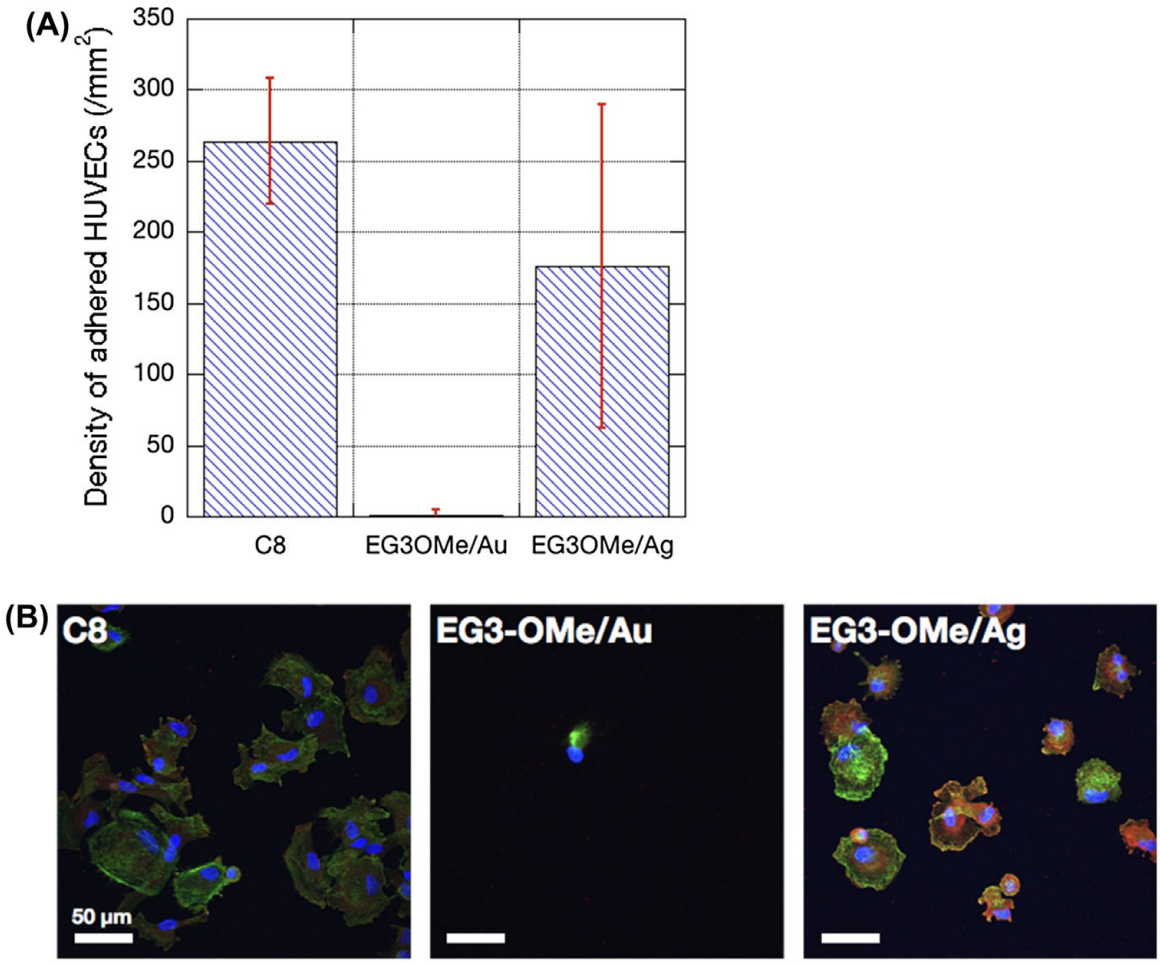

Figure 3. (A) Density of adhered HUVECs on C8, Au- and Ag-supported EG3-OMe SAMs (n = 15). (B) Fluorescent microscope images of HUVECS adhered on the SAMs.

the C8 and Ag-supported EG3-OMe SAMs. Together with the red signal from vinculin, HUVECs on these SAMs formed focal adhesion on the substrate and strongly adhered to the SAMs. On contrary, the HUVECs adhered on the Au-supported EG3-OMe SAM remained a spherical shape with small foot print areas, indicating that the Au-supported SAM does not allow HUVECs to form of focal adhesion points.

The adhesion of the HUVECs to artificial materials is governed by specific molecular recognition between an integrin and RGD moieties of the scaffolding protein. In our assay, the monolayers were immersed in serum solution for 12 h, and we confirmed that the all SAMs were covered with serum proteins. Our recent analysis by MALDI ToF Mass and QCM-D techniques revealed that there was only small ratio of fibronectin and vitronectin in the scaffolding protein and the conformational changes (denaturation) was suppressed on the Au-supported SAM [32]. This result indicates that the scaffolding protein on the Au-supported SAMs did not provide the binding sites (RGD moieties).

3.2. Surface force operating between the SAMs in PBS solution

As discussed above, we found out that the bioinertness of the Au-supported EG3-OMe SAM is high different from the Ag-supported one. The next question is the underlying the mechanism governing the bioinertness of the Au-supported EG3-OMe SAM. To answer this question, we performed surface force measurements for these SAMs to investigate the interfacial behaviors of molecules near the monolayers. Force–distance curves measured between the SAMs in PBS (pH7.4) were displayed in Figure 4. An attractive force was observed between the C8 SAMs at distances smaller than 15 nm. By considering the working distance of the attraction, the attraction is attributed to van der Waals and hydrophobic forces [33]. In the case of the Ag-supported EG3-OMe SAM, the attraction worked at separations smaller than

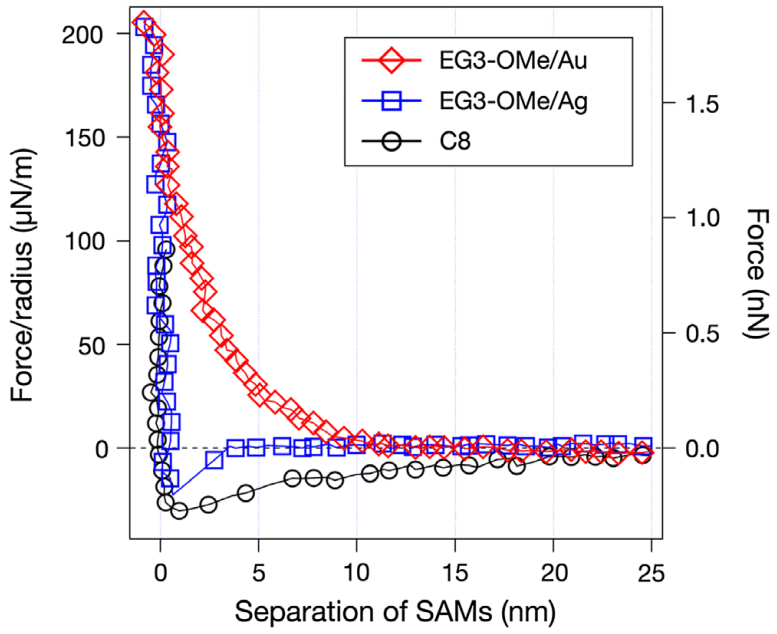

Figure 4. Force–separation curves recorded on an approach for symmetric systems of the SAMs (same SAMs prepared for both probe and substrate) in PBS solution.
Note: Force was expressed in both nN (force) and μN/m (Derjaguin approximation).

4 nm. This attraction can be attributed not to hydrophobic attraction but only to van der Waals attraction, since hydrophobic attraction cannot be expected from the wettability of the Ag-supported EG3-OMe SAM [18,34].

In contrast to the C8 and Ag-supported SAM, the repulsion was observed between the Au-supported SAMs at separation smaller than 10 nm. Considering the decay length of the repulsion (3.1 nm), it cannot be attributed to DLVO force (electric double layer force), since the Debye length of the solution is about 0.7 nm. Previously, we reported that bioinert (resistant to fibrinogens and platelet cells) OEG SAMs are commonly covered by a layer of interfacial water molecules, whose structure and dynamics are different from those in bulk region [18]. The water layer plays a role of a physical barrier against biomolecules and cells, and there is clear correlation between bioinertness and the presence or absence of the water-induced repulsion. The correlation was obviously reproduced also in this work. Therefore, we conclude that the interfacial water with a thickness of about 5 nm (half of the working distance of the repulsion) play a role of the physical barrier deterring fibrinogen and serum proteins from the adsorption, resulting in the inertness to platelet cells and HUVECs.

3.3. OH stretching modes of water molecules in the vicinity of the SAMs measured by SEIRA spectroscopy

Next, we discuss the difference in the physicochemical states of interfacial water in the vicinity of the SAMs. The spectra in an O–H stretching region reflect the degree of water–water (hydrogen bonding and number of hydrogen bonds per molecule) and water–SAM

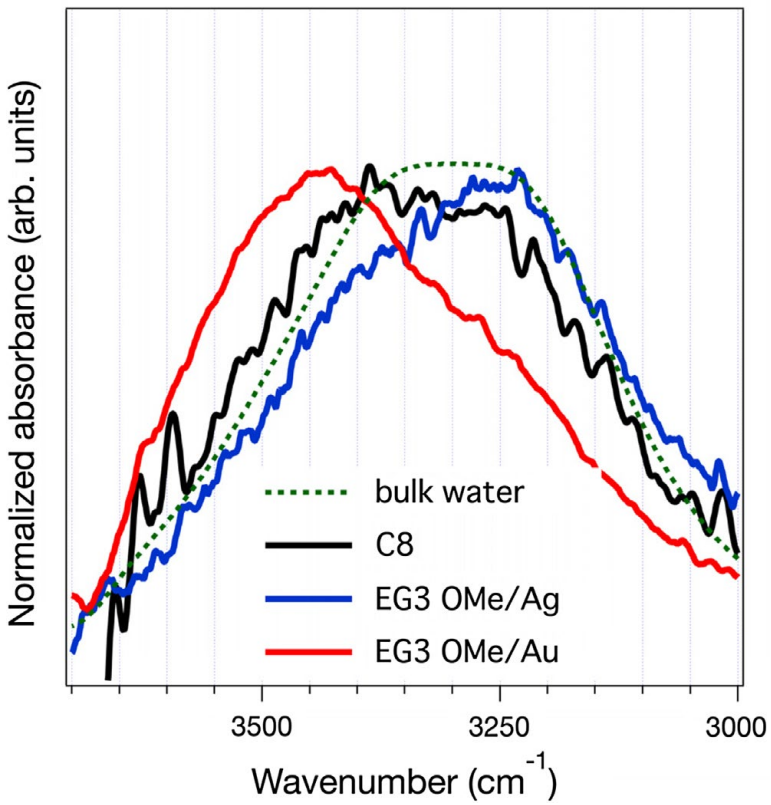

Figure 5. IR absorption spectra in OH stretching region obtained from the SEIRA measurements of water-SAMs interfaces.

Notes: Note that the intensities are normalized simply by the maximum values in the region of OH stretching modes (3000–3800 cm^{-1}), since the enhancement factors for the Au- or Ag-coated prisms are different.

interaction. The spectra measured with the C8, Au- and Ag-supported EG3-OMe SAMs exhibited clear difference from the spectrum of the bulk water. Considering that the decay length for the intensity of the local enhanced magnetic field is about 5 nm [35], which is much larger than the molecular length of the thiolates, these results indicates that the network of hydrogen bonds in the interfacial region is modulated by the SAM–water interactions.

A broad peak of symmetric and asymmetric OH stretching modes consists of a mixture of multiple states of OH bonds. A strong intermolecular interaction is considered to induce a red shift of the peak. As to the assignment of OH stretching modes, we refer the readers to an article by Kitadai et al. [36]. The spectrum for the C8 SAM shows sharp peaks at from 3600 to 3700 cm^{-1}. The peaks in this region were assigned to the OH stretching modes of isolated OH bonds usually observed for water vapor. Water molecules cannot form hydrogen bonds with hydrophobic methyl groups of the C8 SAM, resulting in the isolation of OH bonds from hydrogen bond at the interface. This finding is in agreement with previous results on OH stretching band of water in contact with hydrophobic surfaces studied by sum-frequency generation spectroscopy [37]. In contrast, there is no peak assigned to the OH stretching modes of the isolated OH bond for Ag-supported SAM. This is rationalized by the fact that the EG3-OMe SAMs are more hydrophilic than the C8 SAM, consistent with the trend in the water-induced force discussed before.

The spectrum for the Au-supported EG3-OMe SAM is obviously different from the spectra for the C8 and Ag-supported SAMs. From large population of water molecules with higher frequency region (>3400 cm^{-1}), we assume that interfacial water molecules are in a state of weak hydrogen bonding. Pertsin et al. reported that water molecules penetrate into the Au-supported EG3-OMe SAM with low packing density, whereas the Ag-supported SAM with high packing density does not allow the penetration of water into the SAM. In the case of the Au-supported SAM, the oxygen atoms in the EG chains strongly trap the water molecules via hydrogen bonding. Their results also suggest that one EG3-OMe thiolate accommodates one water molecule in average and half of the penetrating water molecules and a half of the molecules are involved in double hydrogen bonds bridging the EG3-OMe thiolates. The penetrated water provides hydrogen bonding sites (hydrogen acceptors) for the water molecules at the SAM-water interface, but the density of the binding sites is lower than that in bulk water at the interface, resulting in the contribution to the intensity at 3450–3600 cm^{-1} (water molecules with weak hydrogen bonds).

In the cases of the C8 and Ag-supported EG3-OMe SAMs, water molecules cannot form strong hydrogen bonds with the SAMs. Then, the interfacial water molecules attempt to maximize the number of hydrogen bonds by themselves, resulting in the larger population at the region of 3000–3300 cm^{-1} (water molecules with stronger hydrogen bonds and/or with larger number of bonds per water molecule). This behavior of water is consistent with that found in previous reports [38–40].

To conclude this part, the local SAM-water interaction modifies the hydrogen bond state of the interfacial water. Combining with the results of our surface force measurements, the thickness of water molecules with the modulated hydrogen bond network extend up to 3–4 nm.

It also should be noted that the spectrum for the Au-supported SAM was very similar to spectra of intermediate water, which is confirmed commonly for platelet compatible polymers such as poly(2-methoxyethyl acrylate) (PMEA), poly(ethylene glycol) (PEG),

and poly(2-methacryloyloxyethyl phosphorylcholine) (PMPC) [41]. In their model, the intermediate water is defined as water molecules bound to a water tightly trapped to polymer chains, and this binding scheme is also same as our model for the water molecules in the vicinity of the Au-supported SAM. We anticipate that a main factor to modulate the state of interfacial water is the intermixing of the EG chains and interfacial water. Smith et al. suggested that the clustering of water molecules is promoted around PEG [42]. It is expected that the clustered water may be a physical barrier to prevent protein adsorption and cell adhesion. The detailed analysis based on *ab initio* calculation is underway.

4. Conclusion

Main conclusions of this work are that the packing density of the EG3-OMe thiolate on a substrate strongly affects the interfacial behavior of water molecules and that the interfacial behavior well correlates with the bioinertness of the monolayers. In this work, we performed the systematic analyses of the interaction of the Au- and Ag-supported EG3-OMe SAMs with fibrinogen, platelet cells, and HUVECs. The Au-supported EG3-OMe exhibited excellent bioinertness, whereas the Ag-supported one allowed their adsorption and adhesion. Our surface force and SEIRA measurements revealed that the hydrogen bonding state of the interfacial water with a thickness of several nm is significantly modulated by the local SAM-water interaction that depends on the molecular packing density. The modulated hydrogen bonding state governs the resulting water-induced force, which directly correlates with bioinertness. We believe that our findings contribute to molecular-level understanding of the role of interfacial water molecules in the adsorption of biological molecules (lipids, proteins, DNA, etc.) onto solid surfaces and self-assembly of them into their higher-order structures [43–45].

Acknowledgements

This article is dedicated to Professor Emeritus Teiji Tsuruta and his family. We would like to express our sincere appreciation to him for his critical and insightful comments and discussions. T.H. acknowledges the financial support of MEXT KAKENHI.

Disclosure statement

No potential conflict of interest was reported by the authors.

Funding

This work was financially supported by the MEXT [grant number 26282118]; KAKENHI [grant number 15KK0184].

References

[1] Lasseter TL, Clare BH, Abbott NL, et al. Covalently modified silicon and diamond surfaces: resistance to nonspecific protein adsorption and optimization for biosensing. J Am Chem Soc. 2004;126:10220–10221.

[2] Bolduc OR, Masson JF. Monolayers of 3-mercaptopropyl-amino acid to reduce the nonspecific adsorption of serum proteins on the surface of biosensors. Langmuir. 2008;24:12085–12091.
[3] Ekblad T, Liedberg B. Protein adsorption and surface patterning. Curr Opin Colloid Interface Sci. 2010;15:499–509.
[4] Lopez GP, Albers MW, Schreiber SL, et al. Convenient methods for patterning the adhesion of mammalian-cells to surfaces using self-assembled monolayers of alkanethiolates on gold. J Am Chem Soc. 1993;115:5877–5878.
[5] Hayashi T, Hara M. Nonfouling self-assembled monolayers: mechanisms underlying protein and cell resistance. Curr Phys Chem. 2011;1:90–98.
[6] Jeon SI, Andrade JD. Protein surface interactions in the presence of polyethylene oxide. 2. Effect of protein size. J Colloid Interface Sci. 1991;142:159–166.
[7] Jeon SI, Lee JH, Andrade JD, et al. Protein surface interactions in the presence of polyethylene oxide. 1. Simplified theory. J Colloid Interface Sci. 1991;142:149–158.
[8] Love JC, Estroff LA, Kriebel JK, et al. Self-assembled monolayers of thiolates on metals as a form of nanotechnology. Chem Rev. 2005;105:1103–1169.
[9] Hayashi T, Fricke A, Katsura K, et al. Adsorption state of diethyldisulfide on Au(111) studied with a combined system of HREELS and STM. Surf Sci. 1999;427–428:393–397.
[10] Hayashi T, Kodama C, Nozoye H. Structural evolution of dibutyldisulfide adsorbed on Au(111). Appl Surf Sci. 2001;169:100–103.
[11] Hayashi T, Morikawa Y, Nozoye H. Adsorption state of dimethyl disulfide on Au(111): evidence for adsorption as thiolate at the bridge site. J Chem Phys. 2001;114:7615–7621.
[12] Harder P, Grunze M, Dahint R, et al. Molecular conformation in oligo(ethylene glycol)-terminated self-assembled monolayers on gold and silver surfaces determines their ability to resist protein adsorption. J Phys Chem B. 1998;102:426–436.
[13] Feldman K, Hähner G, Spencer ND, et al. Probing resistance to protein adsorption of oligo(ethylene glycol)-terminated self-assembled monolayers by scanning force microscopy. J Am Chem Soc. 1999;121:10134–10141.
[14] Chan YHM, Schweiss R, Werner C, et al. Electrokinetic characterization of oligo- and poly(ethylene glycol)-terminated self-assembled monolayers on gold and glass surfaces. Langmuir. 2003;19:7380–7385.
[15] Pertsin AJ, Grunze M. Computer simulation of water near the surface of oligo(ethylene glycol)-terminated alkanethiol self-assembled monolayers. Langmuir. 2000;16:8829–8841.
[16] Pertsin AJ, Hayashi T, Grunze M. Grand canonical Monte Carlo Simulations of the hydration interaction between oligo(ethylene glycol)-terminated alkanethiol selfassembled monolayers. J Phys Chem B. 2002;106:12274–12281.
[17] Schwendel D, Hayashi T, Dahint R, et al. Interaction of water with self-assembled monolayers: neutron reflectivity measurements of the water density in the interface region. Langmuir. 2003;19:2284–2293.
[18] Hayashi T, Tanaka Y, Koide Y, et al. Mechanism underlying bioinertness of self-assembled monolayers of oligo(ethyleneglycol)-terminated alkanethiols on gold: protein adsorption, platelet adhesion, and surface forces. Phys Chem Chem Phys. 2012;14:10196–10206.
[19] Hayashi T, Tanaka Y, Usukura H, et al. Behavior of hydroxide ions in vicinity of self-assembled monolayers of alkanethiols on metals. e-JSSNT. 2009;7:601–605.
[20] Kreuzer HJ, Wang RL, Grunze M. Hydroxide ion adsorption on self-assembled monolayers. J Am Chem Soc. 2003;125:8384–8389.
[21] Hayashi T, Wakamatsu K, Ito E, et al. Effect of steric hindrance on desorption processes of alkanethiols on Au(111). J Phys Chem C. 2009;113:18795–18799.
[22] Laibinis PE, Bain CD, Whitesides GM. Attenuation of photoelectrons in monolayers of normal-alkanethiols adsorbed on copper, silver, and gold. J Phys Chem. 1991;95:7017–7021.
[23] Sauerbrey G. Verwendung Von Schwingquarzen Zur Wagung Dunner Schichten Und Zur Mikrowagung. Z Physik. 1959;155:206–222.
[24] Voinova MV, Rodahl M, Jonson M, et al. Viscoelastic acoustic response of layered polymer films at fluid-solid interfaces: continuum mechanics approach. Physica Scripta. 1999;59:391–396.

[25] Hutter JL, Bechhoefer J. Calibration of atomic-force microscope tips. Rev Sci Instrum. 1993;64:1868–1873.
[26] Herrwerth S, Eck W, Reinhardt S, et al. Factors that determine the protein resistance of oligoether self-assembled monolayers – internal hydrophilicity, terminal hydrophilicity, and lateral packing density. J Am Chem Soc. 2003;125:9359–9366.
[27] Li L, Chen S, Jiang S. Protein interactions with oligo(ethylene glycol) (OEG) self-assembled monolayers: OEG stability, surface packing density and protein adsorption. J Biomater Sci, Polym Ed. 2007;18:1415–1427.
[28] Li L, Chen S, Zheng J, et al. Protein adsorption on oligo(ethylene glycol)-terminated alkanethiolate self-assembled monolayers: the molecular basis for nonfouling behavior. J Phys Chem B. 2005;109:2934–2941.
[29] Sivaraman B, Latour RA. The relationship between platelet adhesion on surfaces and the structure versus the amount of adsorbed fibrinogen. Biomaterials. 2010;31:832–839.
[30] Sivaraman B, Latour RA. Time-dependent conformational changes in adsorbed albumin and its effect on platelet adhesion. Langmuir. 2012;28:2745–2752.
[31] Tanaka M, Mochizuki A, Shiroya T, et al. Study on kinetics of early stage protein adsorption on poly(2-methoxyethylacrylate) (PMEA) surface. Colloids Surf A. 2002;203:195–204.
[32] Hayashi et al. in preparation.
[33] Ishida N, Kusaka Y, Ushijima H. Hydrophobic attraction between silanated silica surfaces in the absence of bridging bubbles. Langmuir. 2012;28:13952–13959.
[34] Vogler EA. Structure and reactivity of water at biomaterial surfaces. Adv Colloid Interface Sci. 1998;74:69–117.
[35] Kamata T, Kato A, Umemura J, et al. Intensity enhancement of infrared attenuated total reflection spectra of stearic-acid langmuir-blodgett monolayers with evaporated silver island films. Langmuir. 1987;3:1150–1154.
[36] Kitadai N, Sawai T, Tonoue R, et al. Effects of ions on the OH stretching band of water as revealed by ATR-IR spectroscopy. J Solution Chem. 2014;43:1055–1077.
[37] Wei X, Shen YR. Vibrational spectroscopy of ice interfaces. App Phy B-Lasers Opt. 2002;74:617–620.
[38] Gragson DE, McCarty BM, Richmond GL. Ordering of interfacial water molecules at the charged air/water interface observed by vibrational sum frequency generation. J Am Chem Soc. 1997;119:6144–6152.
[39] Strazdaite S, Versluis J, Backus EH, et al. Enhanced ordering of water at hydrophobic surfaces. J Chem Phys. 2014;140:054711.
[40] Strazdaite S, Versluis J, Bakker HJ. Water orientation at hydrophobic interfaces. J Chem Phys. 2015;143:084708.
[41] Morita S, Tanaka M, Ozaki Y. Time-resolved in situ ATR-IR observations of the process of sorption of water into a poly(2-methoxyethyl acrylate) film. Langmuir. 2007;23:3750–3761.
[42] Smith GD, Bedrov D, Borodin O. Molecular dynamics simulation study of hydrogen bonding in aqueous poly(ethylene oxide) solutions. Phys Rev Lett. 2000;85:5583–5586.
[43] Jackman JA, Tabaei SR, Zhao ZL, et al. Self-assembly formation of lipid bilayer coatings on bare aluminum oxide: overcoming the force of interfacial water. ACS Appl Mater Interfaces. 2015;7:959–968.
[44] Jackman JA, Zan GH, Zhao ZL, et al. Contribution of the hydration force to vesicle adhesion on titanium oxide. Langmuir. 2014;30:5368–5372.
[45] Kanayama N, Sekine T, Ozasa K, et al. Terminal-specific interaction between double-stranded DNA layers: colloidal dispersion behavior and surface force. Langmuir. 2016;32:13296–13304.